NANOFILTRATION OF CIP WATERS FROM IODINE X-RAY CONTRAST MEDIA PRODUCTION: PROCESS DESIGN AND MODELLING

Drews, Anja*[1]; Klahm, Thorsten[1]; Renk, Berit[1]; Saygili, Mahmut[2]; Baumgarten, Goetz[3]; Kraume, Matthias[1]
* corresponding author: Tel.: +49-30-314 72687, Fax: +49-30-314 72756,
E-mail address: a.drews@vt.tu-berlin.de
[1] TU Berlin, Institut für Verfahrenstechnik, Sekr. ACK 7, Ackerstr. 71-76, D-13355 Berlin
[2] Schering AG, Müllerstr. 178, D-13353 Berlin
[3] Amafilter Deutschland GmbH, Am Pferdemarkt 11, D-30853 Langenhagen

Abstract

CIP (cleaning in place) waters from X-ray contrast material production cause considerable disposal costs as for discharge of iodine-containing effluents a legal limit of only 1 ppm AOX has to be met. Therefore, CIP waters which typically contain more than 1000 ppm are currently incinerated, thus requiring a huge energetic effort. A two-stage nanofiltration process consisting of an enrichment and a purification step was designed for separating contrast agents out of rinsing waters. Required areas for both stages were exemplarily calculated. Rejection was greater than 99% at transmembrane pressures of 20-40 bar and resulting fluxes of up to 200 L/(m²h). Besides designing an economically feasible nanofiltration process which yields a permeate with concentrations below the legal limit and a retentate of much less volume for incineration, the aim of this project was to further application of mathematical model descriptions of NF transport phenomena and to find an appropriate design equation. It could be shown that in this case concentration polarisation or gel layer formation were of minor importance. As adsorption appeared to cause the principal resistance to both solvent and solute flux, parameters of an extended solution-diffusion-model were fitted in such a way that they account for this physical effect.

Keywords: nanofiltration, iodine X-ray contrast medium, process design, modelling, adsorption

1. Introduction

CIP waters from X-ray contrast agents production give rise to considerable disposal costs. The standards for wastewater discharge in Germany are set under the Federal Water Act [1] whereby any discharge of wastewater requires a licence. The German water laws are a collective term for the Länder and federal regulations. The competence as such is with the Länder. In the case of iodine-containing effluents the limiting value is not fixed but subject to individual assay. For the manufacturing plant of concern in this study it was set to 1 ppm AOX (i.e. 3.6 ppm AOI). CIP waters from X-ray contrast agents production which typically contain more than 1000 ppm are often incinerated, thus requiring a huge logistic and energetic effort. Due to their application, contrast media have to be biologically inert and are therefore practically non-biodegradable [2]. Alternative treatment processes include UV-promoted destruction of the molecules leading to unknown by-products which in turn may cause environmental problems. Evaporation on the other hand is highly energy consuming. Therefore, a purely physical process with lower energy consumption shall be employed.

By screening for suited membranes at varying operating parameters such as temperature, transmembrane pressure and retentate concentration a membrane filtration process was to be

designed to separate contrast agents out of rinsing waters. The aim was to find an economically feasible enrichment factor and to design a nanofiltration process which yields a permeate with concentrations below the legal limit and a retentate of much less volume for incineration. In order to further physical understanding of membrane transport phenomena and to find a design equation a suitable model description was sought. Besides molecular weight polarity and charge of the molecules are important parameters influencing interaction with the membrane and therefore retention [3]. The possibility of describing NF by a universal model has been discussed by Straatsma et al. [4] but was found to be unlikely. They set up a NF model based on the Maxwell-Stefan transport equations but concluded that fitted parameters lost their physical meaning as they contradicted literature values but instead compensated for phenomena not included in the model. It has to be noted that they did not consider concentration polarisation. In contrast, a semi-empirical approach was employed here. For prediction of flux and rejection this requires only little information such as feed concentration and transmembrane pressure and thereby enables easy practical application. On the other hand, it only holds for the investigated membrane/solute/solvent combination. The influence of concentration polarisation is discussed.

2. Theory

Transport through RO and NF membranes is often described by the solution-diffusion-model (SDM). For dilute salt solutions, this consists of two equations for transport of solvent or permeate *P* and solute *j* through the membrane [5,6].

$$\dot{m}_P = A \cdot \left(\Delta p - \Delta \pi \right) \tag{1}$$

$$\dot{m}_j = B \cdot \left(c_{jF} - c_{jP} \right) \tag{2}$$

(with $\dot{m}_w \approx \dot{m}_P$ since $\dot{m}_w >> \dot{m}_j$)

Since each solvent/solute/membrane combination is different, parameters *A* and *B* need to be fitted to experimental data. As the basic SDM only describes transport through the membrane and does not consider additional resistances it generally overestimates flux. In addition to solution and diffusion, however, other phenomena such as concentration polarisation, gel-layer formation or adsorption can occur which make further modifications necessary.

2.1. Concentration polarisation

Concentration polarisation arises as a concentration gradient is established when solute molecules are retained at the surface of the membrane. Assuming steady state and Fick's law a differential mass balance yields [5,6]:

$$\frac{c_{jM} - c_{jP}}{c_{jF} - c_{jP}} = \exp\left(J_P \cdot \frac{\delta}{D_j} \right) \tag{3}$$

Applying the film theory [7] the unknown thickness δ can be replaced by the mass transfer coefficient *k* which can be calculated from common Sherwood correlations.

$$k = \frac{D_j}{\delta} \tag{4}$$

For spiral wound modules, Schock [8] suggested the following equation (see also [9,10] for a comprehensive review of *Sh* correlations):

$$Sh = 0.065 \cdot Re^{0.875} \cdot Sc^{0.25} \tag{5}$$

$$Sh = \frac{k \cdot d_h}{D} \tag{6}$$

$$Re = \frac{w \cdot d_h}{\nu} \tag{7}$$

$$Sc = \frac{\nu}{D} \tag{8}$$

$$v = \frac{\dot{V}}{A_{eff}} = \frac{\dot{V}}{l \cdot d_{ch} \cdot \varepsilon} \tag{9}$$

Besides viscosity and diffusitivity, geometrical features of the feed channel and spacer such as porosity ε and hydraulic diameter d_h must be known to apply this equation. These, however, may not always be readily available.

As will be seen permeate concentration c_{jP} is negligible in this case, thereby reducing Eq. (3) to

$$\frac{c_{jM}}{c_{jF}} = exp\left(\frac{J_P}{k}\right). \tag{10}$$

2.2. Adsorption

Adsorption onto surfaces is commonly described by Langmuir or Freundlich equations which express the amount of adsorbed molecules in terms of the surrounding concentration. Here, a Freundlich isotherm is used:

$$\frac{c_{j,ads}}{c_{j,ads,max}} = a \cdot c_{jF}^{n} \tag{11}$$

3. Experimental

3.1. X-ray Contrast Media

X-ray contrast media are injected during X-ray examination to provide visual contrast of otherwise non-absorbing tissues and organs. Absorption of X-rays is facilitated by elements of high atomic number such as iodine and barium. Derivatives of 2,4,6-triiodobenzoic acid are the most commonly used X-ray contrast agents. They can be of either ionic or non-ionic form with molecular weights ranging from approx. 600 - 1600 g/mol [11]. In 1996, 360t of iodine X-ray agents were prescribed in Germany, 90% of which were non-ionic [2].

CIP waters from different contrast agents (of both ionic and non-ionic forms) production lines are typically collected in a common storage tank. In order to minimise the number of experiments one representative substance each was selected for screening experiments. In addition experiments were carried out with mixtures.

Concentration was measured using UV-spectroscopy (Specord 200, Analytik Jena). At 245 nm, the relationship between absorbance and concentration was found to be linear up to 35 mg/L. Samples containing more were accordingly diluted with de-ionised water. All concentrations are given in g iodine/L.

3.2. Membrane Screening

Seven nanofiltration and six reverse osmosis membranes as listed in Table 1 were tested. It should be noted that this classification was made according to manufacturers terminology. Of those, three were selected for further investigations in which transmembrane pressure, temperature and retentate concentration were varied between 20 and 40 bar, 20 and 35 °C, and 0 and 25 g/L, respectively. Membrane screening was conducted in a test cell (effective membrane area 44 cm², Amafilter GmbH) at cross flow velocities of 2.3 m/s. For each run a new sheet was used and some experiments were repeated to ensure reproducibility of results. Retentate and permeate were recycled into the surge tank to avoid time-varying feed concentrations. As feed flow rates were much higher than permeate flow rates the concentration was assumed to be constant over the length of the membrane, too ($c_{jF} \approx c_{jR}$). Flux was measured on-line by weighing on a digital scale and recording the signal over time.

Table 1
List of tested membranes

Membrane type	**Manufacturer**
NF:	
Desal 5 DK	Osmonics
Desal 5 DL	Osmonics
CK	Osmonics
Nitto LES 90	Nitto
NTR 7450	Nitto
N 30	Nadir
NF PES 10	Nadir
RO:	
Nitto LF 10	Nitto
Trisep X20	Trisep
UTC 80	Toray
Desal SG	Osmonics
Desal SE	Osmonics
Desal SC	Osmonics

3.3. Module Experiments

To represent more technically realistic circumstances, 2.5" spiral wound modules (wide spacer, 1.77 m²) were utilised for obtaining design data. In screening experiments, nanofiltration membranes Desal 5DK and 5DL (both by Osmonics) showed the best

performance (compare 4.1.) and were therefore chosen for module experiments. Both are made of polyamide and have a negative surface charge.

Here, too, retentate and permeate were recycled into the surge tank. By stepwise increases in contrast agent content in the feed the maximum possible retentate concentration which still allows an economically feasible permeate flux was determined. Operating parameters such as temperature (20 – 35 °C), transmembrane pressure (20 – 30 bar), and retentate concentration (0 – 70 g/L) were varied. Mathematical modelling was based on module results.

4. Results

4.1. Screening

The non-ionic agent was identified as the more critical substance for membrane filtration as its rejection was lower than that of ionic substances. Therefore, it was chosen as a model substance for further investigations. Fig. 1 shows membrane performance at 40 bar and 20 °C. Almost total rejection of contrast media could be achieved by use of the nanofiltration membranes Desal 5DK, 5DL and Nitto LES 90. Desal 5DK exhibited the highest rejection rates of more than 99.9%. Desal 5DL showed slightly lower rejection but permeability, i.e. flux at equivalent pressures, was generally higher. For pure substances, similar results were achieved using Nitto LES 90, but here rejection decreased for mixtures of different contrast media. Unlike expected, these preliminary investigations proved that all tested RO membranes were less suited for the specific task as they not only showed lower permeate flow rates but also lower retention than the three selected NF membranes. Satisfactory rejection was achieved by the best RO membrane (Nitto LF 10) but flux at the same pressure was lower thus resulting in a higher energy consumption to reach the same goal.

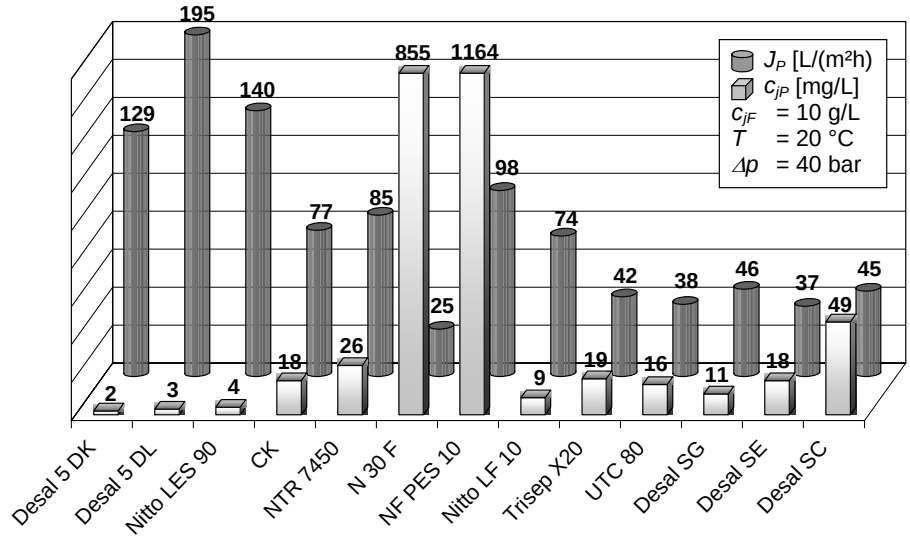

Fig. 1: Exemplary screening results

As temperature increased rejection dropped in all cases due to elevated solute diffusion rates (data not shown). A 20-fold increase in feed concentration did not impair membrane performance. It was observed that rejection increased with feed concentration.

4.2. Process Design

On the basis of module experiments a two-stage process was designed where contrast agents are concentrated in the first stage and the legal limit is met in the second (see Fig. 2). Assuming a feed concentration of 1000 ppm iodine and a rejection of 99.9% (compare Fig. 1, Desal 5DK) the outlet requirements are safely met by this set-up. Even drops in rejection to 99.5%, e.g. due to a decreased flux in technical modules, should be easily dealt with.

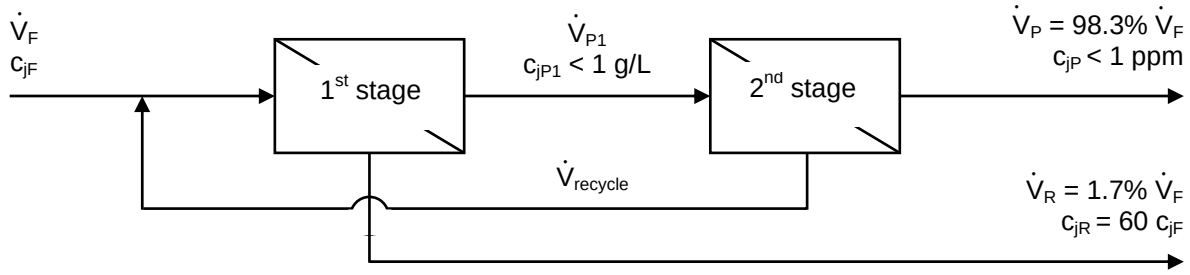

Fig. 2: Two-stage NF-process

Required membrane areas were determined on the basis of the derived model equations for 20 °C on the one hand and based on measured separation characteristics (Fig. 3) for 35 °C on the other. Fig. 3 reveals a common relationship between flux and feed concentration. As concentration was increased, flux decreased due to elevated osmotic pressure, concentration polarisation or other resistances to permeation. At higher temperatures these resistances declined as molecular movement was increased. Fig. 3 also shows that to ensure an economically feasible flux c_{jR} should not much exceed 60 g/L.

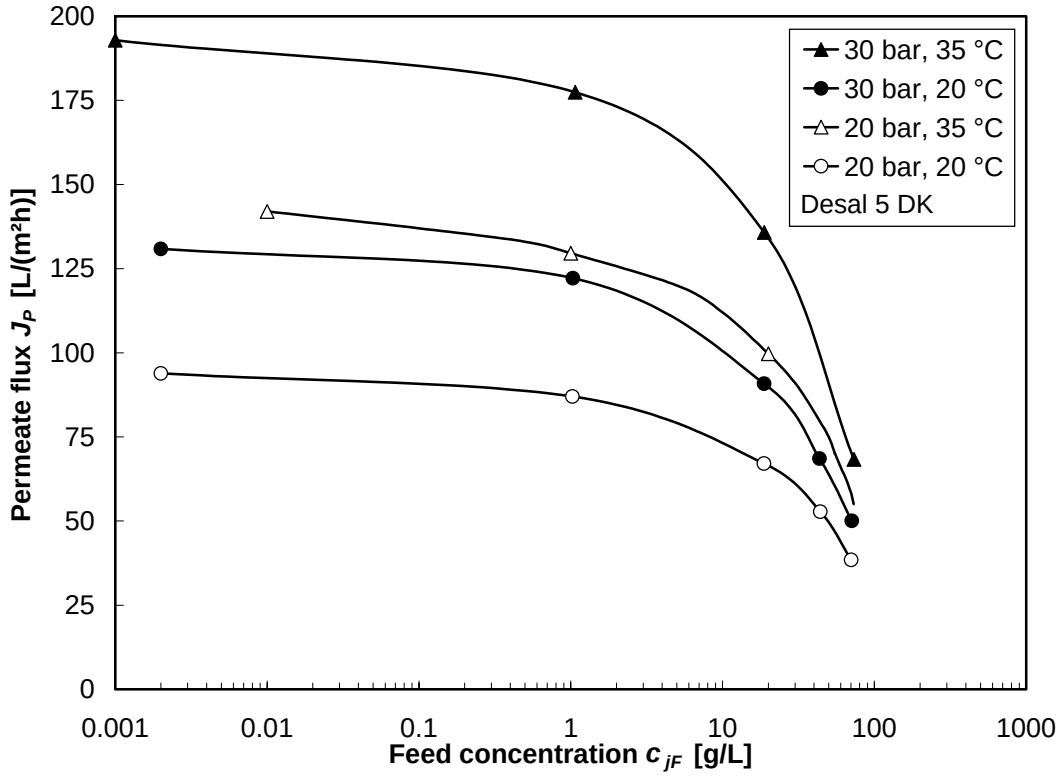

Fig. 3: Separation characteristic of Desal 5 DK at different sets of operating parameters

Both separation characteristics and model equations (see 4.3.) resulted from short-term measurements. Long-term experiments revealed that during operation flux decreased down to approx. 3/4 of the original value due to fouling (data not shown). Therefore, 70% of flux at given conditions was used to estimate the required areas. Considering also that these results were gained using 2.5" modules, flux was halved to represent technical circumstances. In larger modules flux is lower due to longer permeate flow channels and a resulting rise in pressure drop which reduces the driving force. Fig. 4 gives a summary of calculated areas for an assumed feed flow rate of 500 L/h for different sets of operating parameters. Results are given as percentages of the required area at 20 bar and 20 °C.

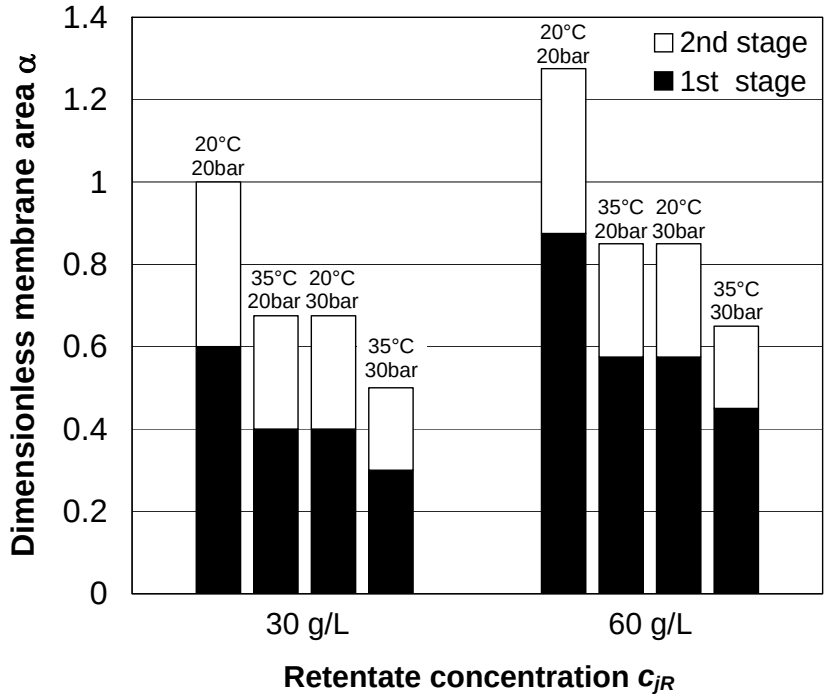

Fig. 4: Calculated minimum areas for different operating conditions as percentages of required area at 20bar and 20°C, c_{jF} = 1 g/L; $\dot{V}_F$ = 500 L/h.

Apart from temperature and transmembrane pressure, retentate concentration c_{jR} can be varied. A rise in c_{jR} results in decreased flux and hence larger area requirements, but permeate yield is increased (Y = 96.7% at c_{jR} = 30 g/L and 98.3% at c_{jR} = 60 g/L). On the other hand, as flux declines retention drops (compare 6a), in the worst case to such an extent that permeate concentration exceeds the legal limit. Therefore, an optimisation of operating conditions should be carried out on the basis of costs for the following:

- transport of concentrate to incineration
- incineration/re-use/reclamation of iodine
- membrane area
- energy

while always ensuring that the 2nd stage permeate concentration falls short of the legal limit. To be on the safe side, process design should be performed for a transmembrane pressure well below the module's maximum operating pressure. This way a pressure increase can still be carried out to counteract a severe flux decline due to changing specifications (e.g. rising retentate concentration).

4.3. Modelling

In the following, modifications to the solution-diffusion-model are derived which hold for transport of a non-ionic contrast medium through Desal 5DK at 20 °C. Initially, focus is laid on flux, and later on rejection to round up the derived model.

4.3.1. Flux

Fig. 5a shows measured flux over transmembrane pressure at different feed concentrations. In contrast to the commonly assumed constant hydraulic permeability a non-linear relationship can be observed even when pure (de-ionised) water is used. This might be caused by membrane compression or by an increased pressure drop on the permeate side at higher flux and a resulting decrease in driving force. In any case A is not constant but depends on Δp which leads to a first modification of Eq. (1):

$$\dot{m}_P = A(\Delta p)\cdot(\Delta p - \Delta\pi) \tag{12}$$

where $\Delta\pi = 0$ for pure water. The correlation for $A(\Delta p)$ takes the form typical for cake filtration with compressible cake or, as in this case, compressible filtration medium:

$$A(\Delta p) = A_0 \cdot \Delta p^{\,m}. \tag{13}$$

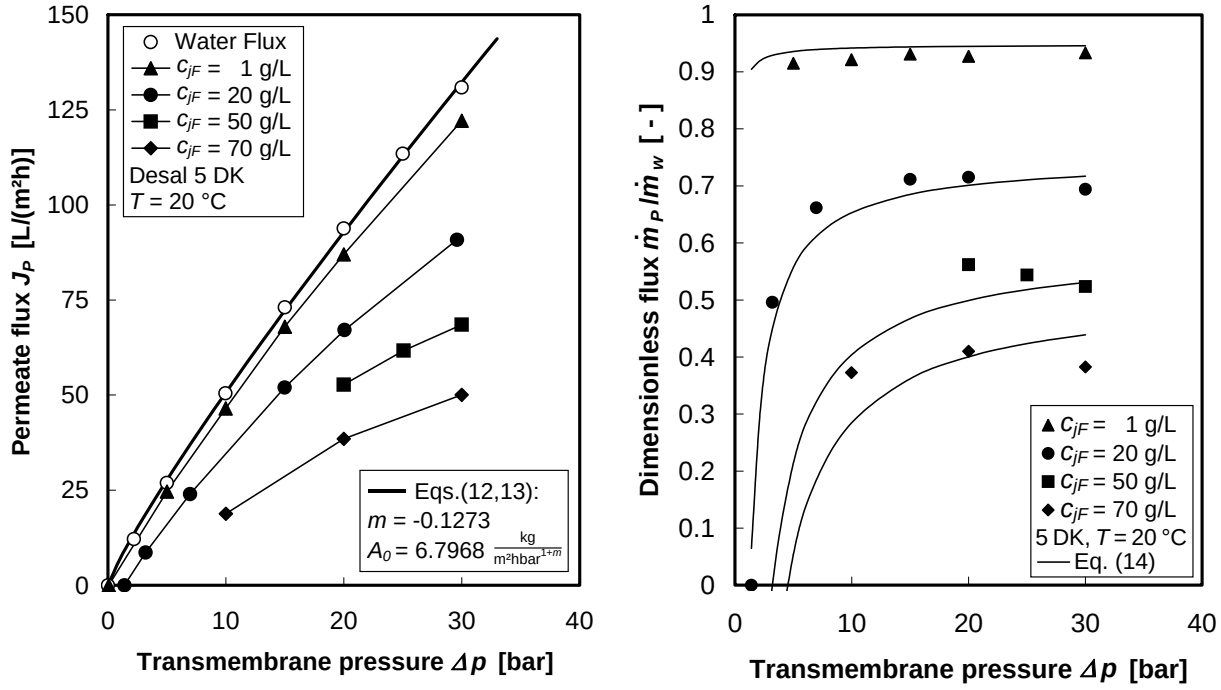

Fig. 5: a) Flux over transmembrane pressure
b) Dimensionless flux over transmembrane pressure, curves calculated from Eq. (14)

In Fig 5a Eqs. (12) and (13) are plotted with fitted parameters A_0 = 6.7968 kg/(m²hbar$^{0.8727}$) and m = -0.1273. As expected, higher feed concentrations gave rise to an increased resistance. To identify this concentration influence a dimensionless flux $\dot{m}_P / \dot{m}_w$ was defined in such a way that permeate flux at a given pressure is divided by the pure water flux at the same pressure. Plotting this dimensionless flux over transmembrane pressure reveals an almost

constant relationship for each feed concentration for pressures greater than approx. 5 bar (see Fig. 5b), i.e. $\dot{m}_P$ can now be described by multiplying pure water flux by a factor $C(c_{jF})$ only depending on feed concentration. In other words, at $\Delta p >> \Delta\pi$ the permeability decrease with pressure is merely caused by the decreasing hydraulic permeability.

$$\dot{m}_P = C(c_{jF}) \cdot A(\Delta p) \cdot (\Delta p - \Delta\pi) \tag{14}$$

For low pressures, however, the otherwise constant dimensionless flux decreases rapidly, highlighting the influence of osmotic pressure which can reach values of up to a few bars for higher concentrations and thus reduces the driving force considerably in this region.

Eq. (14) is plotted in Fig. 5b with $C(c_{jF})$ fitted for each concentration and $\Delta\pi(c_{jF})$ calculated by the van't Hoff equation which proved to be applicable.

$$\Delta\pi = \frac{\Re \cdot T}{\tilde{V}_w} \cdot \xi_{jF} = \Re \cdot T \cdot c_{jF} \tag{15}$$

4.3.2. Rejection

To achieve a satisfactory fit of the complete model Eq. (2) for solute flux must be modified, too. In Fig. 6a full lines represent c_{jP} as calculated from Eq. (2) with B = 0.013 L/(m²h), where a good match for values at 20 g/L is found. Permeate concentrations at higher feed concentrations, however, are overestimated when this value is used (smaller c_{jF} vice versa). This means that B, too, depends on c_{jF}.

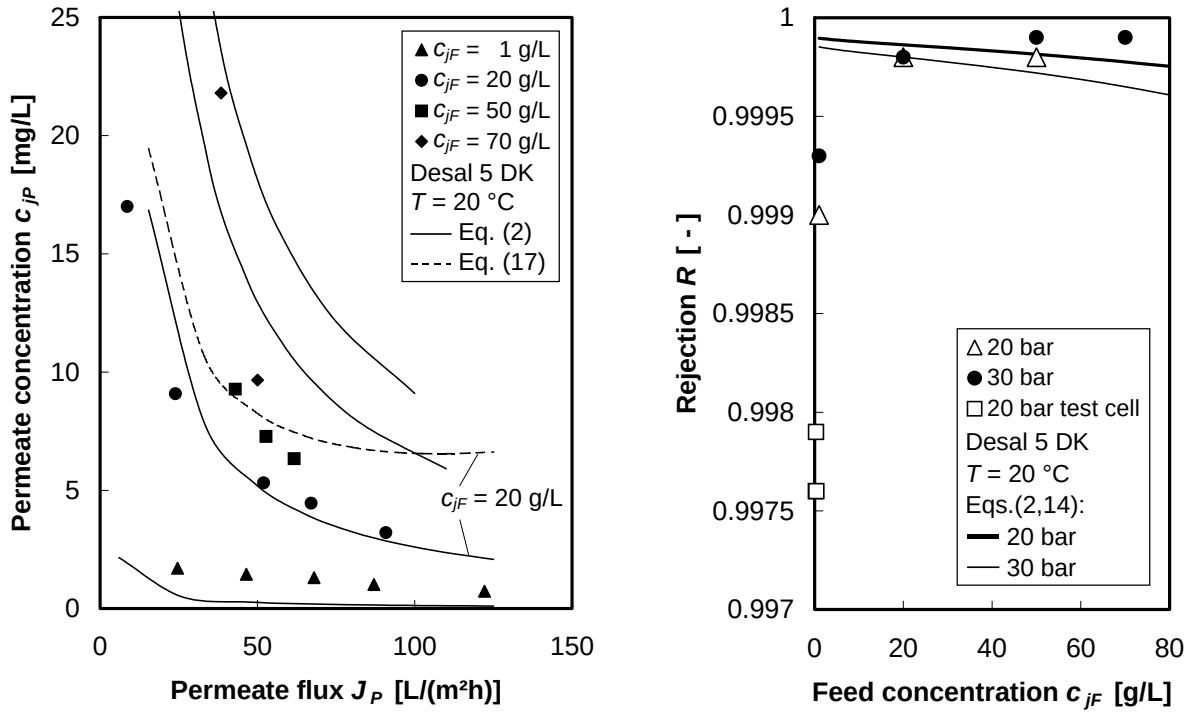

Fig. 6: a) Permeate concentration over flux for different feed concentrations with B = 0.013 L/(m²h), full lines: without concentration polarisation; dotted lines: with concentration polarisation
b) Rejection over feed concentration with B = 0.013 L/(m²h)

Apart from the over- and underestimation of permeate concentration B = const erroneously predicts falling rejection with increasing feed concentration (see Fig. 6b). For $c_{jF} >> c_{jP}$, c_{jF} can be cancelled from the equation for rejection:

$$R = 1 - \frac{c_{jP}}{c_{jF}} = 1 - \frac{\dot{m}_j}{\dot{m}_P \cdot c_{jF}} \cdot \rho_p = 1 - \frac{B}{\dot{m}_P} \cdot \rho_p \tag{16}$$

Thus c_{jF} only influences $\dot{m}_P$ which leads to a decrease of rejection with rising feed concentration. This confirms that B, too, must depend on feed concentration. This dependency must be expressed in such a way that resistance against solute transport rises with increasing feed concentration.

To discuss the influence of concentration polarisation the following module geometry [8] and typical material properties are assumed:

d_h = 1.39 mm
d_{ch} = 1.51 mm
ε = 0.81
l = 0.9 m
ν = 10^{-6} m²/s
D = $1.5 \cdot 10^{-9}$ m²/s

With the experimental flow rate of $\dot{V}_F$ = 1400 L/h the mass transfer coefficient can now be calculated from Eq. (5), yielding k = $3.4 \cdot 10^{-5}$ m/s. According to Eq. (10), e.g. at J_P = 50 L/(m²h) a concentration increase of 50% at the membrane surface occurs for any given feed concentration. The relevant concentration for solute transport through the membrane now is c_{jM} and Eq. (2) changes into:

$$\dot{m}_j = B \cdot \left(c_{jM} - c_{jP} \right) . \tag{17}$$

Eq. (17) implies a linear relationship between c_{jM} and c_{jP} as shown in the following equation:

$$c_{jP} = \frac{\dot{m}_j}{J_p} \approx \frac{B}{J_p} \cdot c_{jM} \tag{18}$$

(with $\dot{m}_j \approx B \cdot c_{jM}$ since $c_{jM} >> c_{jP}$)

Therefore, concentration polarisation at J_P = 50 L/(m²h) yields a 50% increase in permeate concentration for each feed concentration, too. This resulting shift towards higher permeate concentrations at increasing flux (see dotted line in Fig. 6a), however, means falling resistance with rising flux and does not explain the concentration dependency of B.

Another possible effect is adsorption which was observed in an experiment specifically carried out to detect its presence. Feed concentration was suddenly increased from 0 to 0.5 g/L. At this low level osmotic pressure is negligible. This was done at a low level of Δp (here 5 bar) to additionally avoid the effect of concentration polarisation. A flux decline can now only be attributed to adsorption [12,13]. As can be seen in Fig. 7, flux decreased from 25.8 to 25 L/(m²h).

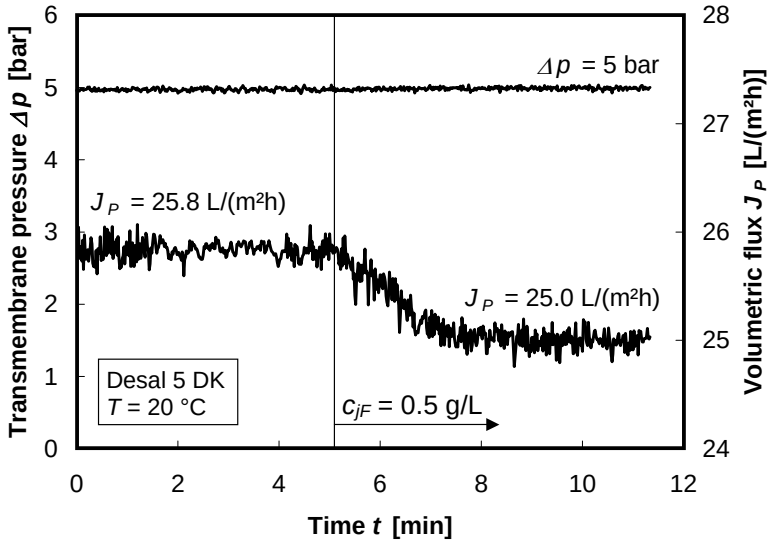

Fig. 7: Flux decline during adsorption experiment

This observation led to the idea of representing $C(c_{jF})$ by a term analogical to a Freundlich adsorption isotherm (Eq. (11)). Introducing this into Eq. (14) yields a common equation for solvent flux with adsorption resistance. The factor *a'*, however, is not identical with the Freundlich coefficient *a* as otherwise zero flux would result for maximum adsorption which would defy any physical explanation.

$$\dot{m}_P = A_0 \cdot \Delta p^m \cdot \left(1 - a' \cdot c_{jF}^n\right) \cdot \left(\Delta p - \Delta \pi\right) \tag{19}$$

As discussed earlier, it was observed that solute flux did not decrease linearly with feed concentration as suggested by Eq. (2) but that instead the solute permeability *B* decreased with rising feed concentration. A physical explanation could be that adsorbed molecules screen off further molecules due to their polarity. In this case, solute permeability would be inversely proportional to the amount of adsorbed molecules. This led to the following implementation of the same Freundlich-type term:

$$\dot{m}_j = \frac{B_0}{a' \cdot c_{jF}^n} \cdot \left(c_{jF} - c_{jP}\right) \tag{20}$$

In Fig. 8 Eqs. (19) and (20) are plotted with fitted parameters:

A_0 = 6.7968 kg/(m²hbar$^{0.8727}$)
a' = 0.0014 (mg/L)$^{-0.538}$
B_0 = 0.00007 L/(m²h)
m = -0.1273
n = 0.524

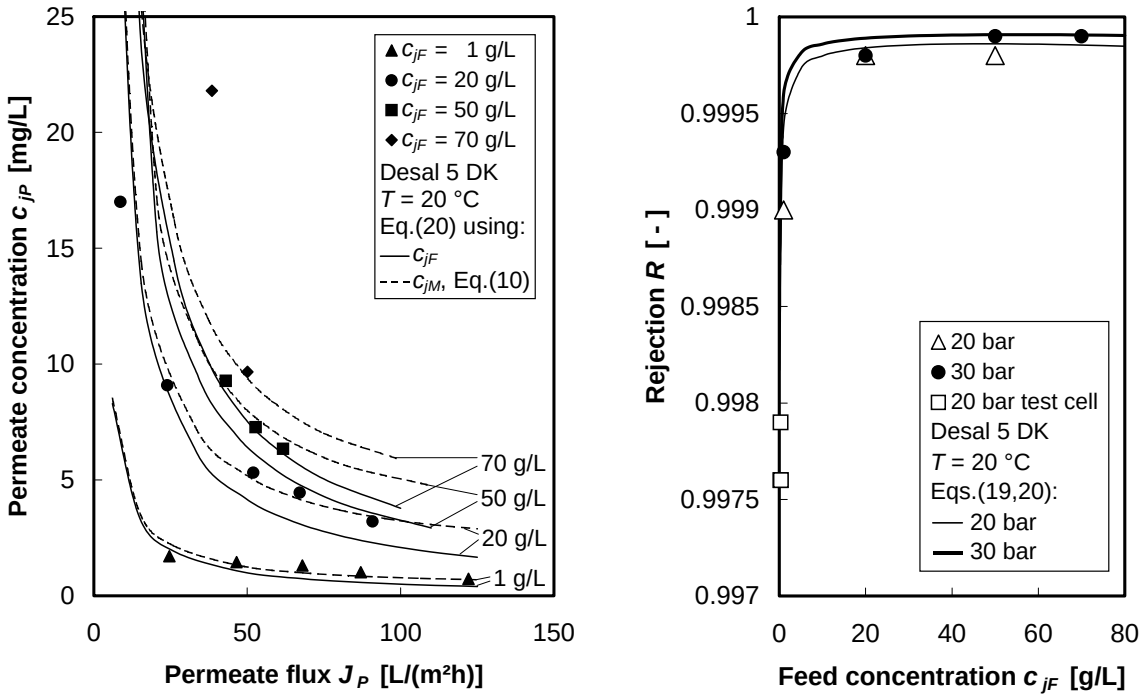

Fig. 8: Results of the complete solution-diffusion model including adsorption, Eqs. (19, 20)
a) Permeate concentration over flux for different feed concentrations; full lines: without concentration polarisation, model using c_{jF}; dotted lines: with concentration polarisation, model using c_{jM} from Eq. (10) and $k = 3.4 \cdot 10^{-5}$ m/s
b) Rejection over feed concentration

Experimental data are well represented by the derived model equations. This means that as transport can be modelled with an implemented Freundlich-type equation adsorption indeed seems to cause a significant mass transfer resistance to both solvent and solute flux.

Including c_{jM} in the model (dotted lines) yields a better match of the curve shape but as discussed earlier requires knowledge of the mass transfer coefficient k.

These equations, however, only hold for T = 20 °C. For rising temperatures, the derived model would erroneously predict decreasing flux because so far it contains temperature only in the osmotic pressure term. Osmotic pressure rises with increasing temperature leading to a higher resistance especially at low transmembrane pressures. Temperature-dependency of both diffusion and adsorption has so far not been implemented.

5. Conclusions

A two-stage NF process consisting of an enrichment and a purification step was designed for cleaning of CIP-waters from iodine X-ray contrast agents production. Rejection of solute decreases with flux and feed concentration but was always greater than 99%. Mass transport through the membrane can be described by an extended solution-diffusion-model. The effect of concentration polarisation is discussed. To account for a significant resistance against both solvent and solute transfer an adsorption isotherm was implemented and parameters fitted to represent experimental data. In order to find out if adsorption really prevails, the adsorption isotherm should be measured and compared with results gained here. Also, further experiments at different temperatures are necessary to validate this assumption and to account for temperature-sensitive processes such as adsorption and diffusion within the model.

List of Symbols

a	Freundlich coefficient	$[(mg/L)^{-n}]$
a'	adsorption factor	$[(mg/L)^{-n}]$
A	solvent permeability	$[kg/(m^2hbar)]$
A_0	coefficient in Eq. (13)	$[kg/(m^2hbar^{1+m})]$
B	solute permeability	$[L/(m^2h)]$
B_0	solute permeability	$[L/(m^2h)]$
c	concentration	$[kg/m^3]$
C	factor in Eq. (14)	[-]
d	diameter	[m]
D	diffusion coefficient	$[m^2/s]$
J	volumetric flux	$[L/(m^2h)]$
k	mass transfer coefficient	[m/s]
l	length of membrane cushion	[m]
m	exponent in Eq. (13)	[-]
$\dot{m}$	mass flux	$[kg/(m^2h)]$
n	Freundlich exponent	[-]
Δp	transmembrane pressure	[bar]
R	rejection	[-]
$\Re$	gas constant	[J/(molK)]
Re	Reynolds number	[-]
Sc	Schmidt number	[-]
Sh	Sherwood number	[-]
t	time	[s]
w	velocity	[m/s]
Y	yield	[-]

Greek symbols

α	dimensionless membrane area	[-]
ε	spacer porosity	[-]
ν	kinematic viscosity	$[m^2/s]$
π	osmotic pressure	[bar]
ρ	density	$[kg/m^3]$
ξ	mass fraction	[kg/kg]

Subscripts

ads	adsorbed
ch	channel
eff	effective
F	feed
h	hydraulic
j	solute
M	membrane surface
max	maximum
P	permeate, solvent
R	retentate
w	water

Acknowledgements

This work was carried out in cooperation with Schering AG and Amafilter GmbH.

References:

[1] Federal Water Act (Wasserhaushaltsgesetz, WHG), Federal Law Gazette I p. 632, 2000.
[2] S. Wischnack, A. Putschew, M. Jekel, Iodierte Röntgenkontrastmittel in Abwässern, Wässern und Trinkwasser, Colloquium Produktionsintegrierte Wasser-/Abwassertechnik, GVC, Bremen 2000.
[3] B. van der Brugge, J. Schaep, D. Wilms, C. Vandecasteele, Influence of molecular size, polarity and charge on the retention of organic molecules by nanofiltration, J. Membr. Sci. 156 (1999) 29-41.
[4] J. Straatsma, G. Bargeman, H.C. van der Horst, J.A. Wesselingh, Can nanofiltration be fully predicted by a model? J. Membr. Sci. 198 (2002) 273-284.
[5] R. Rautenbach, Membranverfahren, Springer-Verlag, Berlin, 1997.
[6] M. Mulder, Basic Principles of Membrane Technology, 2nd Ed., Kluwer Academic Publishers, Dordrecht, 1996.
[7] R.B. Bird, W.E. Stewart, E.N. Lightfoot, Transport Phenomena, Wiley, New York, 1960.
[8] G. Schock, A. Miquel, Mass transfer and pressure loss in spiral wound modules, Desalination 64 (1987) 339-352.
[9] V. Gekas, B. Hallström, Mass transfer in the membrane concentration polarisation layer under turbulent cross flow. Part 1. Critical literature review and adaption of existing Sherwood correlations to membrane operations, J. Membr. Sci. 30 (1987) 153-170.
[10] V.S. Minnikanti, S. DasGupta, S. De, Prediction of mass transfer coefficient with suction for turbulent flow in cross flow filtration, J. Membr. Sci. 157 (1999) 227-239.
[11] W. Krause, H. Miklautz, U. Kollenkirchen, G. Heimann, Physicochemical Parameters of X-Ray Contrast Media, Investigative Radiology, Vol. 29, No. 1 (1994) 72-80.
[12] B. Goers, Spülwassermanagement und Tensidrückgewinnung in Mehrproduktanlagen mit Membranverfahren. PhD Thesis, TU Berlin, 2000.
[13] A. Maartens, P. Swart, E.P. Jacobs, Characterisation technique for organic foulants adsorbed onto flat sheet UF membranes used in abattoir effluent, J. Membr. Sci. 119 (1996) 1-8.